Indentation Test as a Tool for Monitoring the Solidification Process during Injection Molding

V. La Carrubba,[1] W. Gabriëlse,[2] M. van Gurp,[2] S. Piccarolo,[1] V. Brucato[3]

[1]*Dipartimento di Ingegneria Chimica dei Processi e dei Materiali, University of Palermo, Viale delle Scienze, 90128 Palermo, Italy*
[2]*DSM Engineering Plastics, P.O. Box 18, 6160 MD, Geleen, The Netherlands*
[3]*Dipartimento di Ingegneria Chimica ed Alimentare, University of Salerno, Via Ponte don Melillo, 84084 Fisciano (SA), Italy*

ABSTRACT: An inline method for monitoring the solidification process during the injection molding of semicrystalline polymers is demonstrated. The method has been applied to various poly(ethylene terephthalate) (PET) and poly(buthylene terephthalate) (PBT) samples. The technique is based on a simple device by which an additional ejector pin is pushed onto the injection-molded part with a fixed force at different times during the solidification phase while the mold remains closed. The residual deformation (the so-called indentation depth) due to the applied load is measured offline after ejection. By the performance of indentation at different times during the cooling phase, an indentation depth profile, that is, the residual deformation as a function of time, is obtained. With a simplified solid/liquid two-phase model, the evolution of the solidification front in the mold as a function of the cooling time can be determined from the indentation curve. The obtained experimental results agree well with calculations based on the classical theory of heat penetration. Descriptions of several materials (including PET and PBT) with variations in the molecular weight (PET) have been obtained under different operating conditions (various mold temperatures, holding pressures, and indentation pressures). The results show that the indentation test may be regarded as a powerful tool for monitoring the solidification process during injection molding and, therefore, for optimizing injection-molding processing conditions according to material characteristics. © 2003 Wiley Periodicals, Inc. J Appl Polym Sci 89: 3713–3727, 2003

Key words: injection molding; crystallization; indentation

INTRODUCTION

Injection molding is one of the most widely employed processing techniques for manufacturing plastic parts, being characterized by a high degree of automation, high productivity, and high flexibility. During the injection-molding process of a thermoplastic polymer, the material is subjected to high pressures (essentially during the packing phase), high cooling rates (during the whole process), and high shear and elongational rates (essentially during filling), the combination of all these factors governing the final property distribution across the injection-molded sample. In the injection molding of a semicrystalline polymer, crystallization takes place during solidification/cooling, which strongly influences both the shrinkage of the molded part and the final product properties. Moreover, the crystallization kinetics will strongly determine the time needed for cooling and, therefore, the cycle time of the entire process. For these reasons, there is great interest in the crystallization process during processing. Several approaches exist for investigating these complex phenomena. On the one hand, some researchers have put a great deal of effort into the simulation of the injection-molding process with the aim of predicting the final property distribution.[1–3] Obviously, for the quantitative description of structure development during injection molding, data on the crystallization kinetics under processing conditions are required, but these are hard to obtain. On the other hand, much research has been performed in separate studies of the effects of high cooling rates,[1–6] pressure,[7–18] and flow[19,20] on the crystallization kinetics of various polymeric materials, such as polyethylene,[8,13,14] isotactic polypropylene,[5,7,9,17–22] polyamide 6 and polyamide 66,[4,6,7,23] poly(ethylene terephthalate) (PET),[7,15–16,24] and polybutene 1.[9] These studies provide very useful data and give new insights that sometimes can be used in simulation studies.

Beside this type of research, various experimental devices have been designed and implemented that enable direct monitoring of the solidification process during injection molding. Thomas and Bur[25] constructed an optical sensor for monitoring the injection-molding process. On the basis of the reflected light intensity, information was obtained on the crystallization process during injection molding. Another interesting technique is dielectric spectroscopy, as shown by Guillet et al.[26] Using an instrumented mold with

Correspondence to: V. La Carrubba (lacarrubba@dicpm.unipa.it).

TABLE I
Main Characteristics of the Materials

	η_{rel}[a]	M_n	Glass fiber content (%)
PET low M_w	1.6	19,000	0
PET high M_w	2	33,600	0
PET + glass fiber	1.6	19,000	30
PBT	2.1	22,900	0

[a] Relative viscosity measured in 1% *m*-cresol.

dielectric sensors positioned at the walls of the mold cavity, they detected the dielectric response as a mean, following the progression of the crystallization front inside the mold. In addition, the dielectric response was sufficiently sensitive to identify the successive steps of the closing of the mold, filling, packing, cooling, and ejection of the part. In addition, information concerning the crystallization behavior of the polymer near the wall or close to the center was collected. The gradual filling of the cavity could also be monitored by this method. Finally, Wang et al.[27] and Brown et al.[28] monitored the injection molding of a simple polymer box by ultrasonic waves with the pulse-echo technique. With the help of ultrasound velocity measurements, the solidification process of the part could be monitored during the cooling phase as well as the shrinkage evolution.

In this article, a new inline technique is reported for monitoring the solidification process during injection molding. The method is based on a simple device by which an additional ejector pin is pushed onto the injection-molded part at different times during the solidification phase while the mold remains closed. By the performance of indentation at different times during the cooling phase, an indentation depth profile, that is, the residual deformation as a function of time, can be obtained that gives information about the solidification process. In contrast to the aforementioned methods, this technique does not require sophisticated instrumentation of the mold with dielectric, optical, or ultrasound sensors and detection equipment. The method can easily be implemented with a conventional injection-molding machine without major alterations. Moreover, the ease of operation, the wide applicability to different classes of semicrystalline polymers (polyesters, polyamides, and polyolefins), and

the simplicity of the interpretation make the method very useful for a general understanding of the moldability of a given material in terms of the process cycle time and final properties of the molded part.

The method has been demonstrated on a relatively slowly crystallizing polymer (PET) varying in its molecular weight, a relatively fast crystallizing polymer poly(buthylene terephthalate) (PBT), and a glass-fiber-reinforced system (PET with 30% glass fibers). A simplified two-phase model is proposed for interpreting the experimental data. On the basis of this model, the propagation rate of the solidification front can be derived from the indentation depth experiments. Finally, experimental data are compared with predicted data based on a simple heat-transfer model.

EXPERIMENTAL

Materials

Two unfilled PET samples, a 30% glass-fiber-reinforced PET sample, and a PBT sample were used to illustrate the applicability of the method. The main material characteristics are reported in Table I.

Operating conditions

A conventional injection-molding press was used with the processing conditions reported in Table II. The pressure in the mold was recorded by a pressure transducer, and this led to the pressure traces reported in the Results and Discussion section.

Description of the method

The method was implemented on a standard, multipurpose injection-molding machine under typical operating conditions. A two-cavity mold was adopted, each cavity being rectangular, as shown in Figure 1, which reports the cavity length and width. The cavity thickness was 1.6 mm. In one of the two cavities, 12 mm from the cavity edge and opposite to the gate, a pressure sensor was installed, which allowed the pressure trace in the cavity to be recorded during the process (see Fig. 1).

TABLE II
Operating Conditions Adopted for the Materials

	T_m (°C)	Indentation pressure (bar)[a]	Holding pressure (bar)[b]	Holding time (s)	T_w (°C)
PET low M_w	285	30	30	3.5	135
PET high M_w	285	44	60	5.5	135
PET + glass fiber	288	20, 30, 50	25, 50, 75	2	105, 135
PBT	260	44	45	2.9	90

[a] Pressure values set at the machine. For the equivalent, real pressure multiply by 16 (hydraulic plug to front pin surface ratio).
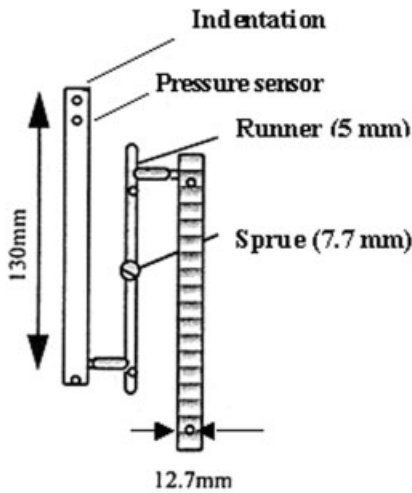[b] Pressure values set at the machine. For the equivalent real pressure, multiply by 13.

Figure 1 Mold used for the indentation test.

In the same cavity, the device used for the indentation test was implemented, consisting of a hydraulically driven piston with a diameter of 4 mm, as sketched in Figure 2. The position of the indentation pin was such that its center was situated 8 mm apart from the cavity edge (see Fig. 1) and close to the pressure sensor.

After the packing phase was completed, the pin was pushed toward the sample surface with a constant pressure, and this caused the pin to penetrate within the polymer. The hydraulic pressure of the circuit driving the indentation pin was kept constant for 2 s and then removed. This time was necessary so that the cold pin would freeze an imprint on the sample. This, after ejection, was used as a measure of the indentation depth. By the performance of the indentation at different times during the cooling phase, a typical indentation depth profile, that is, the residual deformation as a function of the cooling time, could be obtained, as schematically illustrated in Figure 3. The initial point of the curve reported in Figure 3 at time zero represents the maximum indentation depth (δ_{max}) recorded at the end of the packing phase, during which the polymer was predominantly in the molten state. With increasing cooling time, the amount of the solid phase increased. This led to a gradual decrease in the indentation depth, which reached a final value (δ_{min}) at which the material was completely solidified. Note that the indentation depths reported in Figure 3 were measured offline, that is, after the whole cycle had been completed, with a high-precision device.

THEORETICAL BACKGROUND

Before we discuss the results in more detail, we first describe how these curves are interpreted. Furthermore, we describe a simplified model based on classical heat-transfer theory to explain the shapes of the curves and their dependence on both material parameters and processing conditions.

Interpretation of the indentation test

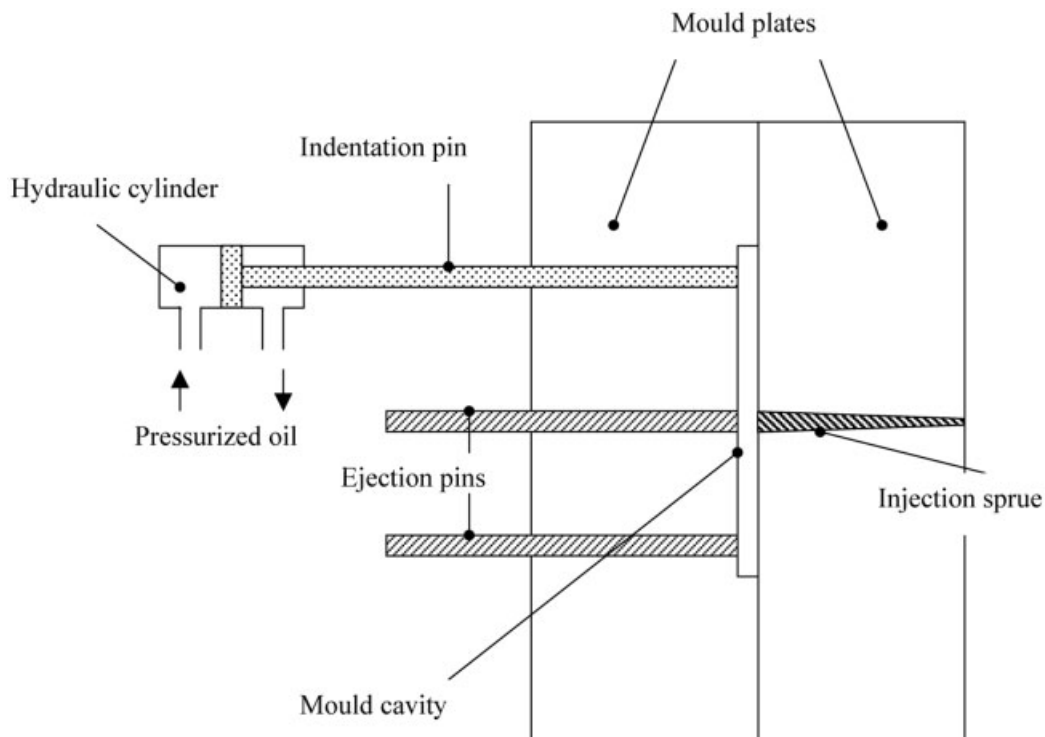A typical curve recorded during an indentation test is shown in Figure 3. After gate sealing, indentation

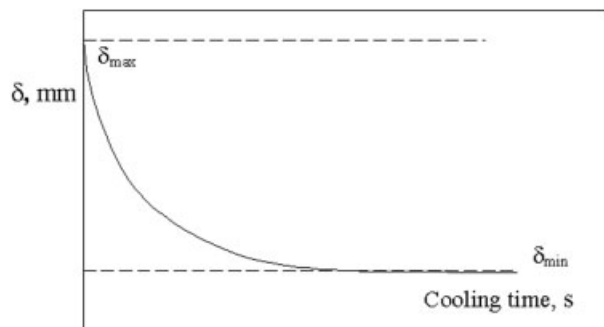**Figure 2** Scheme of the indentation test setup.

Figure 3 Typical shape of the indentation test profile.

causes a change in the volume of the polymer, which occupies the cavity. The main assumptions proposed here are the following:

1. The change in the volume is only determined by the compressibility of the material inside the cavity. Therefore, it is assumed that the solid shear strength contributes only to a negligible extent to the equilibrium end position of the indentation pin, this assumption being supported by the observation that the shear strength is both for the liquid and solid phases much lower than the bulk strength.[29] The indentation depth will then be related to the compressibility of the material inside the cavity.
2. For simplicity, it is assumed that during solidification, the molded sample consists of two phases, a solid crystallized phase and a phase that is still liquid, the total compressibility being a volume-weighted average of the compressibility of both phases.

A schematic drawing including all the details necessary for the interpretation of the test is reported in Figure 4 [δ is the indentation depth (residual deformation), P_i is the indentation pressure, P_h is the holding pressure at the time of indentation, l is the half-thickness of the cavity, and x is the thickness of the solid layer]. If one assumes that gate freeze-off has taken place within the holding pressure step (i.e., no more material can flow back to the runner during indentation), mass conservation can be assumed during indentation. In general, the infinitesimal change in volume [$dV(T,P)$] is a function of temperature and pressure:

$$dV(T, P) = \left(\frac{\partial V}{\partial T}\right)_P dT + \left(\frac{\partial V}{\partial P}\right)_T dP \qquad (1)$$

The relative change in the sample volume is given by

$$\frac{dV(T, P)}{V(T, P)} = \frac{1}{V}\left(\frac{\partial V}{\partial T}\right)_P dT + \frac{1}{V}\left(\frac{\partial V}{\partial P}\right)_T dP = \varepsilon dT - \beta dP$$

$$(2)$$

where $\varepsilon = 1/V(\partial V/\partial T)_P$ is the coefficient of thermal expansion and $\beta = -1/V(\partial V/\partial P)_T$ is the compressibility. If we further assume that the indentation process of the pin up to its end position is very rapid (i.e., almost isothermal), this implies that almost no temperature change will occur during the indentation, that is, $dT = 0$. More precisely, although there is a transverse temperature distribution in the mold during the cooling phase, this hypothesis states that the temperature distribution does not dramatically change during the indentation time. This apparently crude assumption is justified by the observation that during the 2 s adopted for the application of the indentation pressure, only a small fraction determines the penetration depth (dependent on the compressibility of the two-phase system). Most of such a time
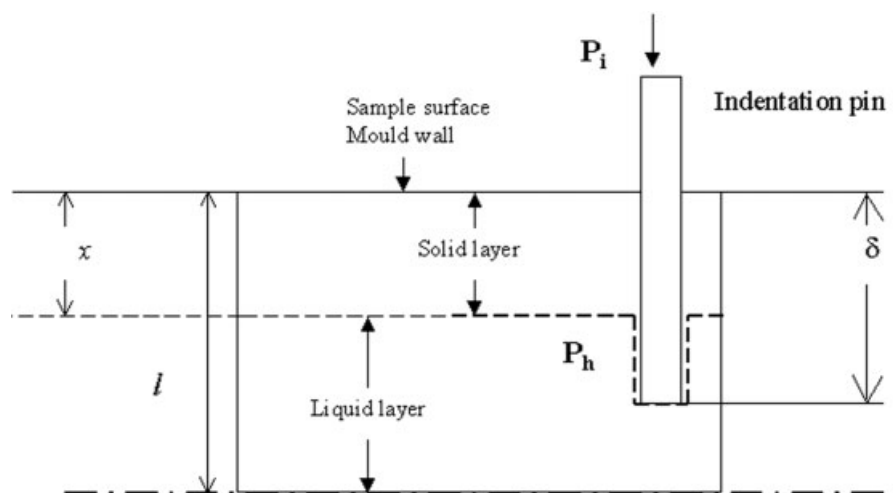

Figure 4 Schematic drawing of the indentation test. Only half of the cavity is reported because of the symmetry of the problem.

interval is necessary for consolidating a measurable imprint after ejection.

By integrating eq. (2) from state $[V_1, P_1]$ (before indentation) to state $[V_2, P_2]$ (after indentation), we get

$$\int_1^2 \frac{dV}{V} = \ln\left(\frac{V_2}{V_1}\right) = -\int_{P_1}^{P_2} \beta(T, P)\, dP \quad (3)$$

Equation (3) implies that the change in the sample volume depends on the compressibility of the material and on the applied pressure.

Because the sample may be regarded as a two-phase system, liquid and solid, we can rewrite eq. (3) for the solid and liquid phases:

$$\left(\frac{V_2^S}{V_1^S}\right) = \exp\left(-\int_{P_1}^{P_2} \beta_S(T, P)\, dP\right) = A_S \quad (4)$$

$$\left(\frac{V_2^L}{V_1^L}\right) = \exp\left(-\int_{P_1}^{P_2} \beta_L(T, P)\, dP\right) = A_L \quad (5)$$

where V^S and V^L are the volumes of the solid and liquid phases, respectively; β_S is the compressibility of the solid; and β_L is the compressibility of the liquid. Note that both A_S and A_L are functions of time because they are both functions of temperature and pressure, which, in turn, are functions of time. Equations (4) and (5) describe the change in the volume for each phase as a result of the indentation. V_1 and V_2 can be defined as follows:

$$V_1 = V_{1S} + V_{1L} \quad (6)$$

and

$$V_2 = V_{2S} + V_{2L} \quad (7)$$

The volumetric solid fraction (x_S) is then defined as follows:

$$x_S = x_S(t) = \frac{V_{1S}}{V_1} = 1 - \frac{V_{1L}}{V_1} \quad (8)$$

From eqs. (4)–(8), we get

$$V_{2S} = V_{1S}A_S = A_S x_S V_1 \quad (9)$$

$$V_{2L} = V_{1L}A_L = A_L(1 - x_S)V_1 \quad (10)$$

Then, by adding eq. (9) to eq. (10), we have

$$V_2 = A_L(1 - x_S)V_1 + A_S x_S V_1 \quad (11)$$

The change in the volume due to indentation is proportional to the indentation volume:

$$V_2 = V_1 - \delta S \quad (12)$$

where S is the cross section of the indentation pin. By equating the right-hand terms of eqs. (11) and (12), we get:

$$A_L(1 - x_S)V_1 + A_S x_S V_1 = V_1 - \delta S \quad (13)$$

Therefore, it is possible to relate the solid fraction to the measured indentation depth:

$$x_S = \frac{[V_1 - A_L V_1] - \delta S}{A_S V_1 - A_L V_1} \quad (14)$$

It should be kept in mind that the solid fraction does not vary during the indentation time, as the portion of the indentation time determining $\delta(t)$ is short in comparison with the thermal transient. By means of eq. (14), it is possible to evaluate the solid fraction at time t at which the indentation is performed. In fact, x_S is a function of δ, A_S, and A_L, which, in turn, are functions of time. Equation (14) can be simplified on the basis of these further assumptions:

1. β_L and β_S are almost constant with T.[30]
2. The integration limits of both coefficients, A_S and A_L, are constant. These integration limits are $P_1 = P_h$ and $P_2 = P_i$. P_i is constant during a series of indentation experiments performed to derive the typical curve reported in Figure 3. As for P_h, it obviously varies from one indentation experiment to another because they are performed at different times during the cooling phase. Nevertheless, the cavity pressure values at which the indentation tests are performed are very low with respect to the indentation pressure (also for the first indentations); this will be clearer when the pressure traces recorded during the indentation tests are shown (see the Results and Discus-

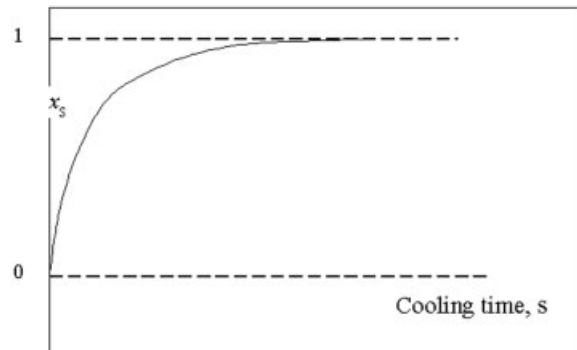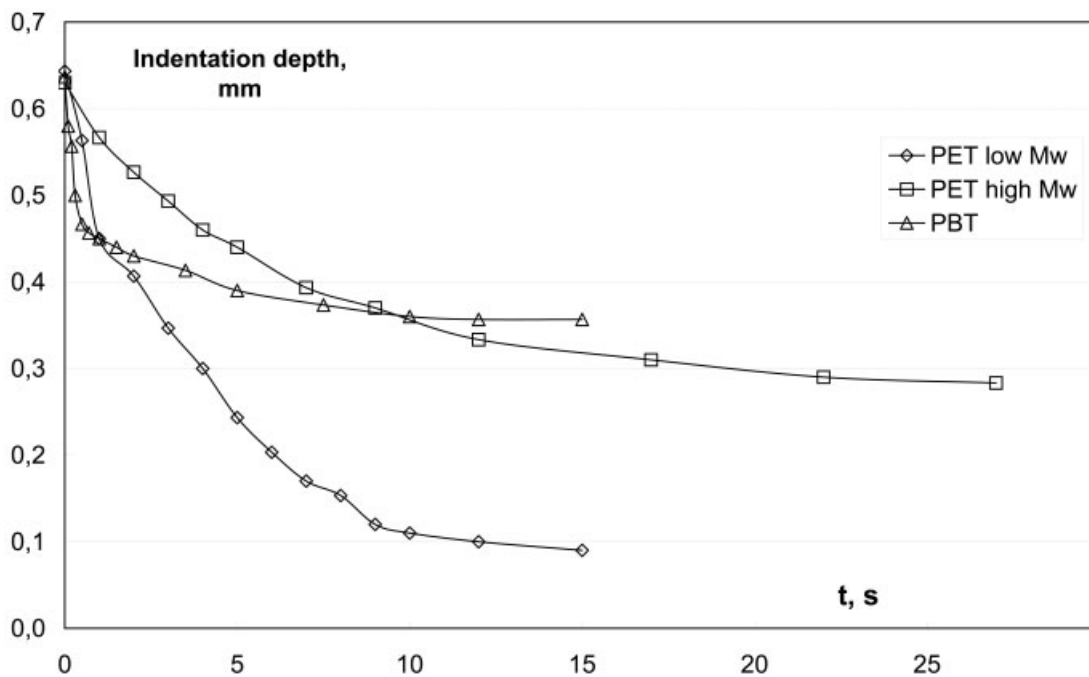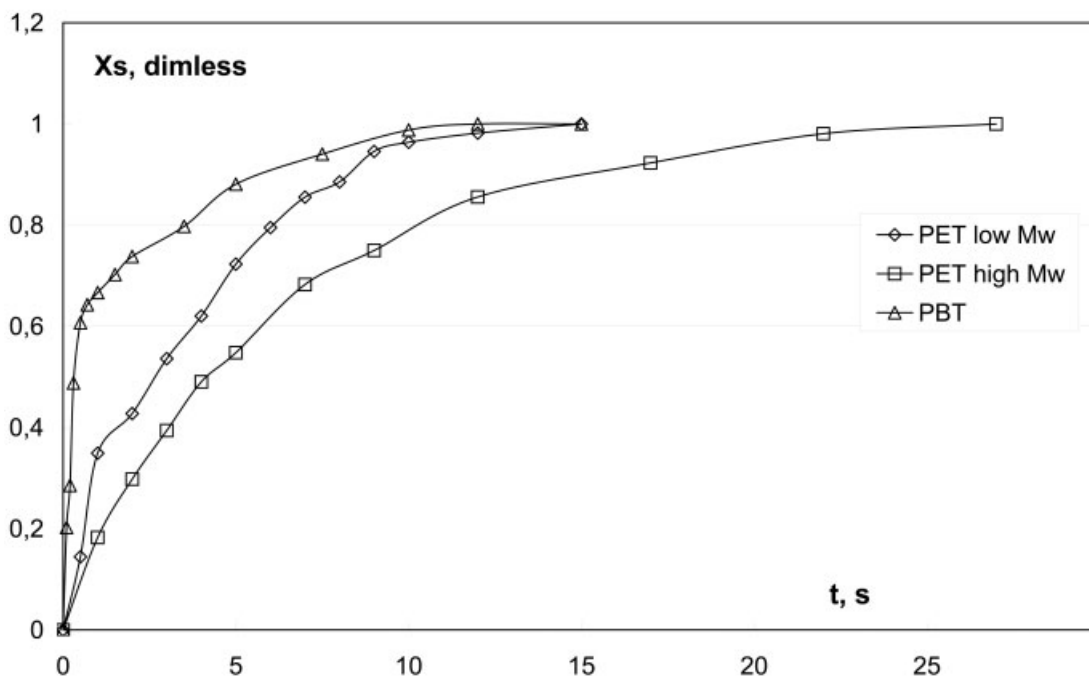**Figure 5** Typical shape of the solid-layer evolution with time as derived from the indentation test profile (see Fig. 3).

Figure 6 (a) Indentation curves recorded for two PET samples and one PBT sample (for the operating conditions, see Table II), (b) normalized curves representing the evolution of the crystallization front (x_S) according to eq. (17), and (c) the indentation depth as a function of the square root of time. Open symbols: region of linear dependence on square root of time. Full symbols: region of deviation from linear dependence.

sion section). Therefore, one may conclude that P_h is constant for the successive indentation tests.

On the basis of assumptions 1 and 2, we can conclude that A_S and A_L are constant during a series of inden-

tation tests performed at different times in the cooling phase. Then, we can consider that

1. For $t = 0$, we have $\delta = \delta_{max}$ (i.e., the indentation depth is maximum) and $x_S = 0$ (i.e., the solid
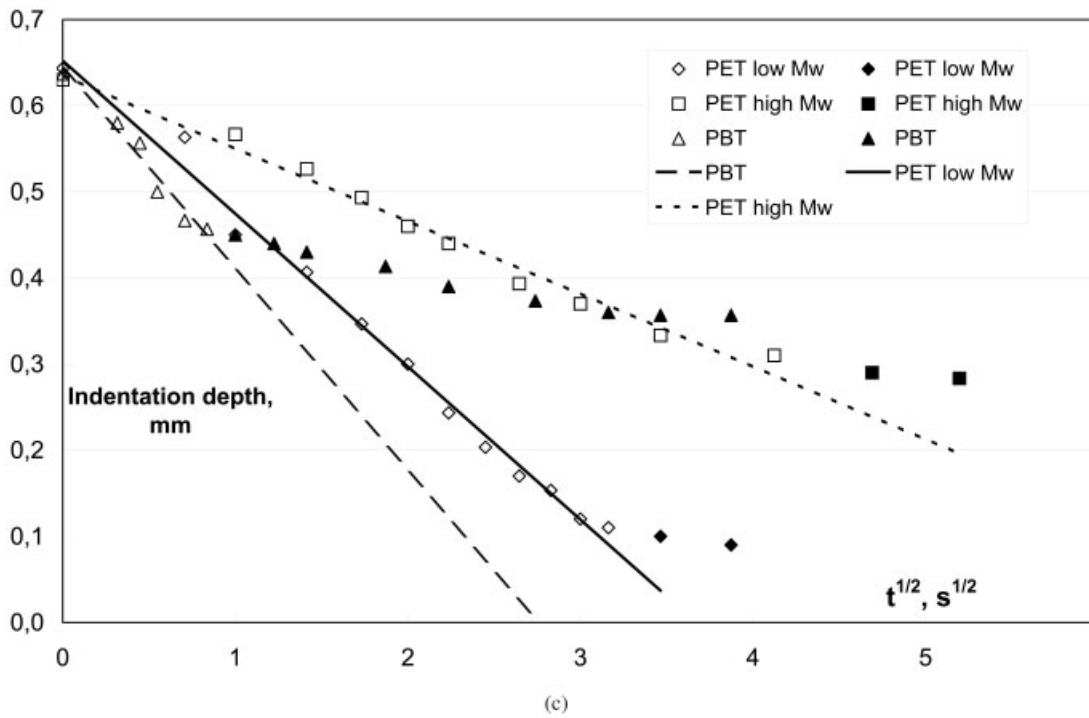
(c)

Figure 6 (*Continued from the previous page*)

fraction is negligible at the beginning of the indentation test). This condition, substituted into eq. (13), gives

$$\delta_{max}S = V_1 - A_L V_1 \qquad (15)$$

2. For $t = \infty$, we have $\delta = \delta_{min}$ (i.e., the indentation depth is minimum) and $x_S = 1$ (i.e., the system is completely solid at the end of the indentation test). This condition, substituted into eq. (13), gives

$$\delta_{min}S = V_1 - A_S V_1 \qquad (16)$$

By combining eqs. (15) and (16) with eq. (13), we obtain

$$x_S = \frac{\delta - \delta_{max}}{\delta_{min} - \delta_{max}} \qquad (17)$$

Therefore, from the curves reporting δ versus time, the typical shape of which is shown in Figure 3, the evolution of x_S as a function of time can be derived with eq. (17), which represents a sort of normalization procedure for working out the solid fraction on the basis of δ_{max} and δ_{min} (proportional to the liquid and solid compressibility, respectively). A typical curve of the solid front position as a function of time drawn from indentation depth profiles is shown in Figure 5. In other words, according to our model, the recorded indentation depth profile actually probes the displacement across the sample thickness of the solidification front as a function of time.

Modeling the solid-layer evolution

A simple model is proposed that predicts the shape of the solid-layer evolution as a function of time, as qualitatively depicted in Figure 5. The model is based on the solution of the transient heat-transfer problem during cooling within the mold. For the sake of simplicity, the heat transfer is schematized by the consideration of a semi-infinite slab. The transient heat transfer, if heat convection is neglected (because we assume that the gate freeze-off has already occurred and only the cooling stage is studied) and a monodimensional geometry is assumed, is governed by the following equation:

$$\frac{\partial T}{\partial t} = \alpha \frac{\partial^2 T}{\partial x^2} \qquad (18)$$

where T is the temperature (K), x is the distance from the cold wall (m), $\alpha = k/(\rho c_p)$ is the thermal diffusivity (m^2/s), k is the thermal conductivity (W/mK), ρ is the density (kg/m^3), and c_p is the specific heat (J/kg K). For the case of interest, a suitable initial condition is the following:

- For $t \leq 0$, $T = T_m$ and $\forall x \geq 0$, T_m being the melting temperature at which the injection is carried out. This condition corresponds to a uniform temperature distribution before the cooling starts. Real conditions approach this situation if the injection speed is high and the holding time is short, as the heat transfer during those stages becomes negli-

gible. Furthermore, it is known that, in transient heat conduction, after a short time the initial temperature distribution does not significantly affect subsequent temperature distributions.[31] Finally, viscous heating counteracts cooling, keeping the initial average temperature of the cooling stage closer to the injection temperature.
- Suitable boundary conditions are the following:

- For $x = 0$, $T = T_w$ and $\forall t > 0$, T_w being the wall temperature (i.e., the mold temperature).
- For $x = \infty$, $T = T_m$ and $\forall t > 0$. This condition corresponds to the fact that very far from the cold wall, the perturbation due to the change of T_w is not sensed; that is, very far from the surface, the temperature is always equal to the initial temperature.

The solution of this problem has the following form:

$$\frac{T_m - T}{T_m - T_w} = erfc\left(\frac{x}{2\sqrt{\alpha t}}\right) \tag{19}$$

erfc is the complementary function of the Gaussian error function:

$$erfc(y) = 1 - erf(y) = 1 - \frac{2}{\sqrt{\pi}} \int_0^y \exp(-y^2)\, dy \tag{20}$$

It may be assumed that solidification or crystallization occurs abruptly at a given crystallization temperature (T_c) with no other requirement from knowledge of crystallization kinetics, since experimental evidence shows that at high cooling rates crystallization occurs in a narrow range of temperatures, this being characteristic of a given polymer.[4–6] This statement finds further support in that a small crystalline fraction is sufficient to give rise to the onset of solidlike behavior, that is, gelation.[32,33] Therefore, we can write

$$\frac{T_m - T_c}{T_m - T_w} = erfc\left(\frac{x}{2\sqrt{\alpha t}}\right) = K \tag{21}$$

where K is a constant value. Then, the relationship between the position at which the solidification front is located and the time at which the solidification occurs is governed by the following equation:

$$\left(\frac{x}{2\sqrt{\alpha t}}\right) = K_1 \tag{22}$$

where K_1 is a constant value (different from K). Equation (22) can be rewritten in the following form:

$$x = (K_1 \times 2 \times \sqrt{\alpha}) \times \sqrt{t} \tag{23}$$

According to eq. (23), a dependence of the position of the solidification front on the square root of time should be expected, and this is at least in qualitative agreement with the first part of the curve shown in Figure 5, as derived from the indentation test profile. In the next section, we show that the dependence on time predicted by eq. (23) is also quantitatively confirmed by our experimental results. Nevertheless, it is obvious that the theory of heat penetration, drawn from the physical hypothesis of the semi-infinite slab, is valid for a finite slab only for short times, during which the center of the slab maintains the initial temperature, not being reached by the temperature perturbation.

In summary, on the basis of eqs. (19)–(23), it is possible to calculate the profile of the solid front propagation as a function of time, the physical parameters influencing that profile being T_c and α. The operating parameters affecting this profile are T_m and T_w. If we remember that

$$x_S = \frac{x}{l} \tag{24}$$

where l is the half-thickness of the injection-molded part, by combining eqs. (23), (24), and (17), we can draw the time dependence of the indentation depth profile as follows:

$$\delta(t) = \delta_{max} + (\delta_{min} - \delta_{max})x_S(t) \tag{25}$$

$$\delta(t) = \delta_{max} + (\delta_{min} - \delta_{max})\left[\frac{K_1 2\sqrt{a}}{l}\right]\sqrt{t} \tag{26}$$

Equation (26) predicts a square-root dependence fo the indentation depth as a function of time. If one plots $\delta(t)$ as a function of the square root of time, one can determine the intercept giving the initial indentation value (δ_{max}) and the slope, which indicate the kinetics
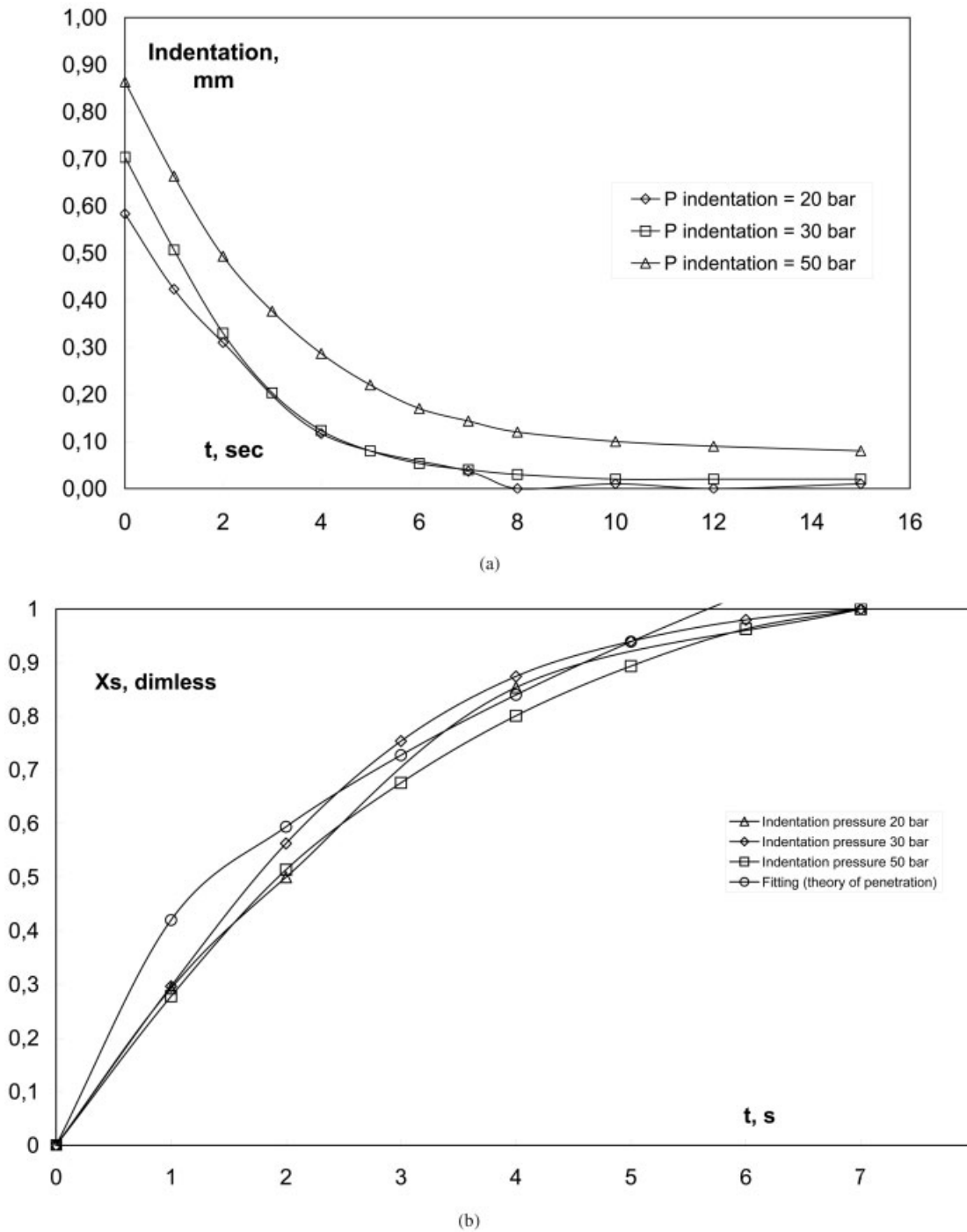
Figure 7 (a) Indentation curves recorded for PET at different indentation pressures and (b) normalized curves representing the evolution of the crystallization front (x_S) together with a theoretical curve based on the heat-transfer model.

of the solidification front propagation. It also should be mentioned that our simplified heat-transfer model gives reasonable results because the convective heat flux can be considered negligible, the first indentation ($t = 0$) being performed during the cooling phase after the gate freeze-off. On the contrary, it was clearly shown by Titomanlio and coworkers[33–35] that the contribution of the heat flux due to convention is highly relevant in the packing phase, in which extra molten polymer is squeezed into the cavity by a high pressure

to compensate for shrinkage taking place with solidification.

RESULTS AND DISCUSSION

Influence of the polymer type and molecular weight

The indentation test profiles [$\delta(t)$] for two PET resins characterized by different molecular weights and for
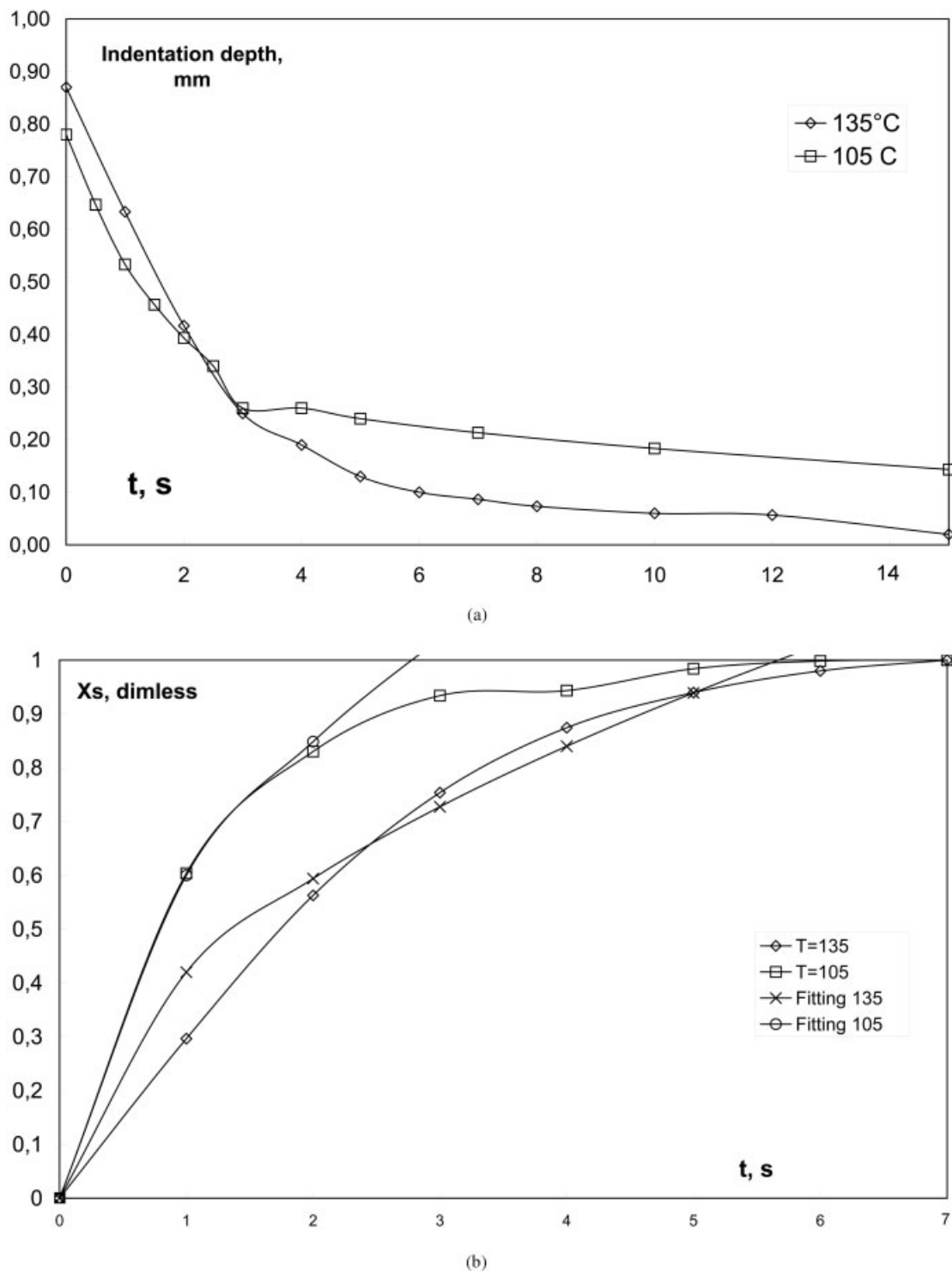
Figure 8 (a) Indentation curves recorded for 30% glass-fiber-reinforced PET at different mold temperatures and (b) normalized curves representing the evolution of the crystallization front (x_S) together with a theoretical curve based on the heat-transfer model.

one PBT are reported in Figure 6(a). The operating conditions are reported in Table II, and the solid-layer evolution as a function of time, as derived from the indentation tests according to eq. (17), is reported in Figure 6(b).

Figure 6(a,b) shows that these three materials have different solidification behaviors. PBT exhibits faster

solidification than the two PET samples, and this is consistent with the general knowledge that PBT is a faster crystallizing polymer than PET.[29] Furthermore, the high-molecular-weight PET exhibits slower solidification than the low-molecular-weight grade, in agreement with the common knowledge that an increase in the molecular weight depresses the crystal-
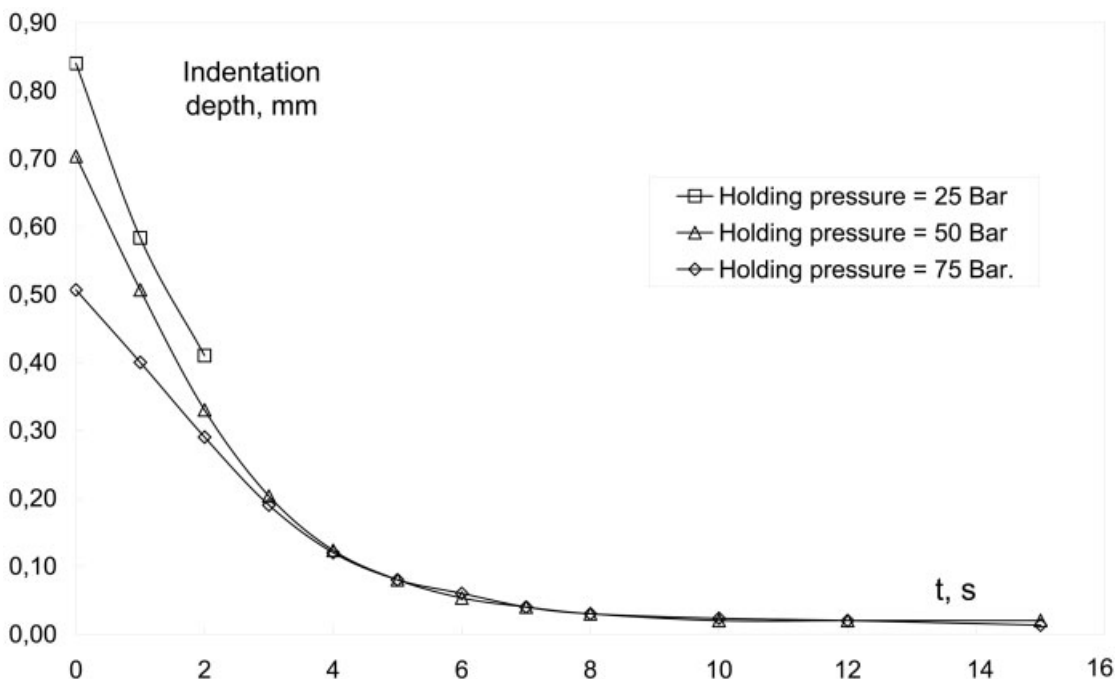
Figure 9 Indentation profiles for different holding pressures for 30% glass-fiber-reinforced PET [indentation pressure (set at the machine) = 30 bar].

lization kinetics.[36] These results show that the indentation test can discriminate between different materials. Such observations are confirmed by the heat-transfer prediction according to eqs. (19)–(26). If one plots the indentation depth as a function of the square root of time, the curves reported in Figure 6(c) are obtained, showing a good agreement (at least for short times) between theoretical expectations (lines) and experimental results (open and full symbols). Several remarks can be stated with reference to the results reported in Figure 6(c). First, the intercept (δ_{max}) corresponds very accurately to the first point of the indentation test profile (at $t = 0$), confirming the reliability of the two-phase model according to which $x_S = 0$ for $t = 0$. Second, the slopes of Figure 6(c) indicate the kinetics of the solidification process, showing that PBT solidifies faster than the low-weight-average-molecular-weight (M_w) PET, which, in turn, solidifies faster than the high-M_w PET. Third, the deviation of the experimental points from the square-root dependence on time (full symbols) starts at a very long time for the slowly crystallizing high-M_w PET, at a very short time for the fast crystallizing PBT, and at an intermediate time for the low-M_w PET. This result shows that the simplified heat-transfer model based on the heat penetration theory (semi-infinite geometry) can predict the solid front propagation more reliably when the solidification process is relatively slow, that is, the more slowly crystallizing the polymer is.

For every indentation test profile, the normalized decrease of the indentation depth for each time step increment Δt can be defined as follows:

$$\delta_{norm}(t) = \frac{\delta_t - \delta_{t+\Delta t}}{\delta_{max} - \delta_{t+\Delta t}} \qquad (27)$$

$\delta_{norm}(t)$ is a monotonously decreasing function of time. We define for our purposes δ_{min} as the value of $\delta(t)$ for time t at which $\delta_{norm}(t)$ is less than 2%; that is: when $\delta_{norm}(t) \leq 0.02$, $\delta(t) = \delta_{min}$. When $\delta_{norm}(t) \leq 0.02$, then $\delta(t) = \delta_{min}$. In this way, the values of δ_{max} and δ_{min} are univocally determined and, from eq. (26), the value of the parameter K_1 can be determined with the typical literature data of α reported in many specialized textbooks of polymers.[29] From the K_1 value, a typical figure of T_c for the polymers studied in this work can be calculated back from eq. (22), the results being reported in Table III. Most interestingly, the calculated values of T_c lie in the typical range of T_c's for PET and PBT, confirming the reliability of the model. Furthermore, the indentation test is able to discriminate between the two PET grades characterized by different molecular weights because they exhibit different crystallization behaviors, which are taken into account for the different T_c values.

Influence of the indentation pressure

Figure 7(a) shows the indentation profiles of a 30% glass-fiber-reinforced PET sample for different values of the indentation pressure, ranging from 20 to 50 bar (see Table II). It appears that the shape of the curve is almost independent of the indentation pressure
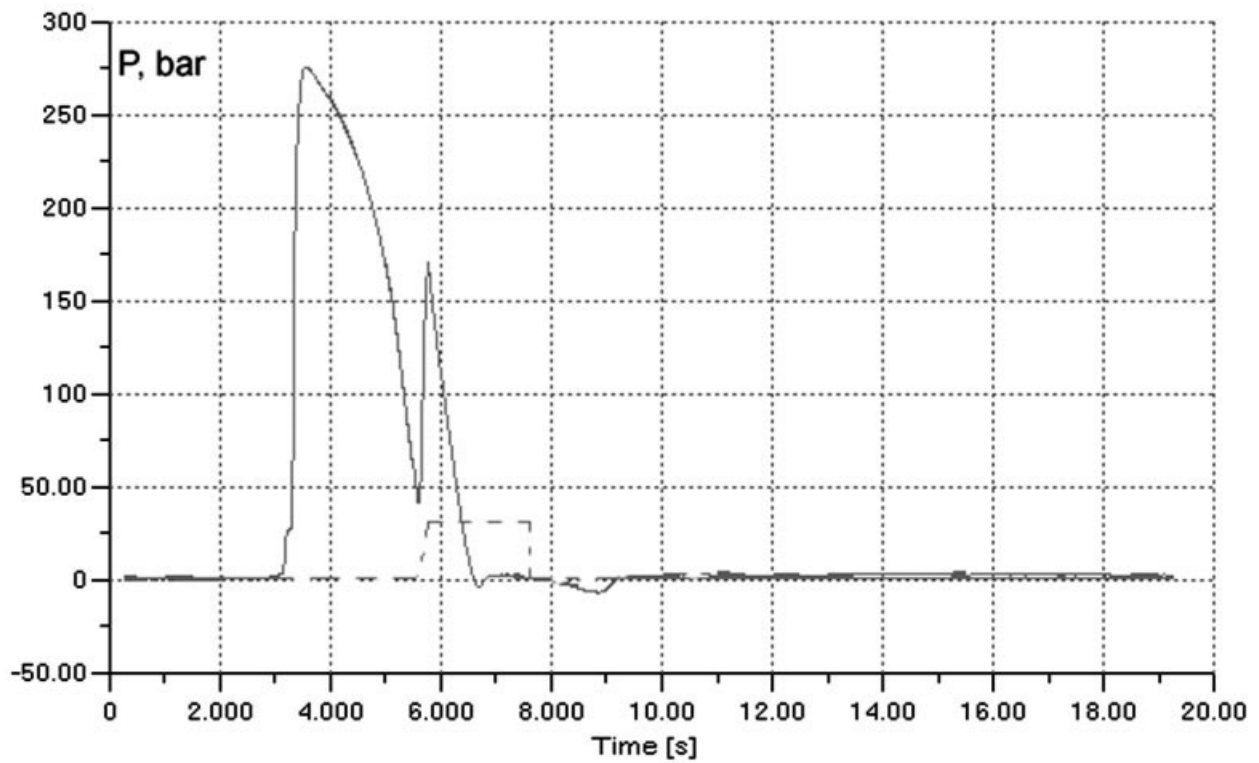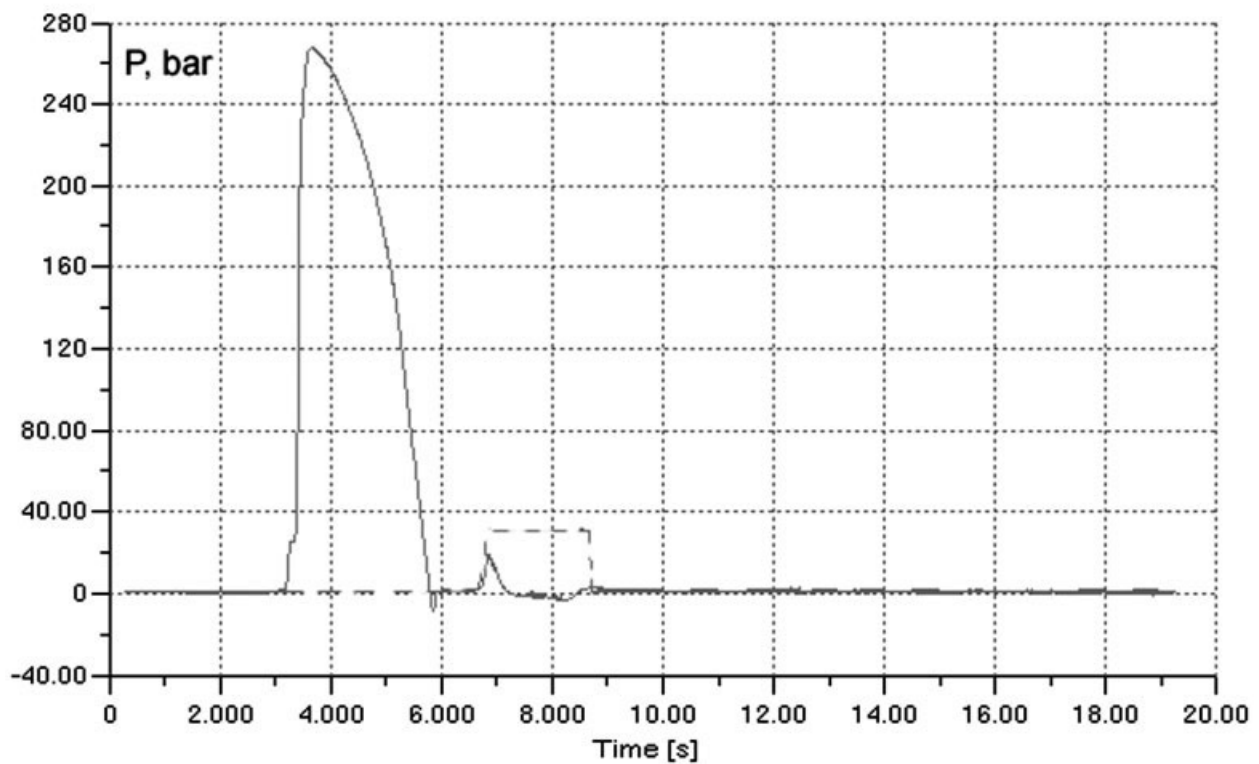
Figure 10 Pressure profiles in the cavity for 30% glass-fiber-reinforced PET at indentation times of (a) 0, (b) 1, and (c) 2 s (indentation pressure = 30 bar, holding pressure = 25 bar).
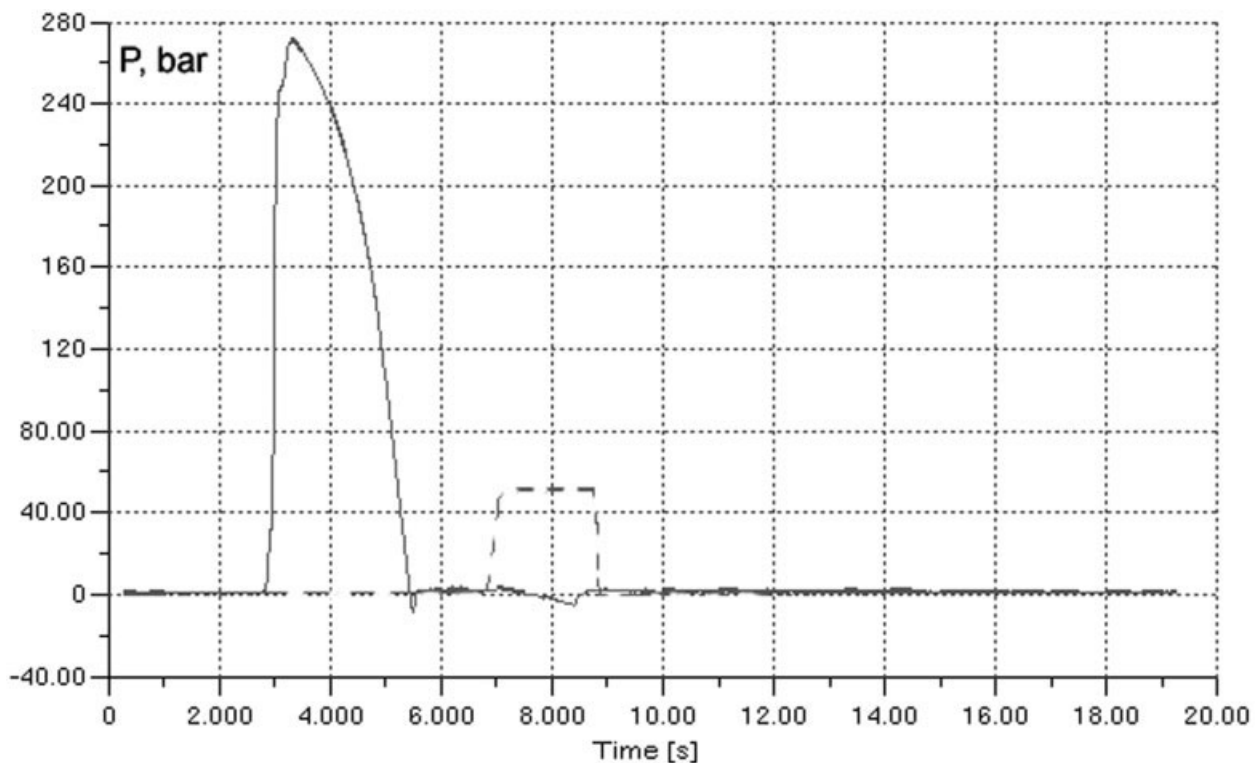
Figure 10 (*Continued from previous page*)

adopted for performing the test. This result is at least in qualitative agreement with the volumetric model here proposed because a variation of the indentation pressure must determine only a shift of the curve along the y axis. Consequently, the solid-layer evolution profiles, as shown in Figure 7(b), are only barely affected by the indentation pressure. This demonstrates that the indentation depth is proportional to the indentation pressure, the compressibility of the system being almost independent of the applied pressure.[30] In any case, the indentation pressure must be at least equal to the pressure of the cavity during the indentation to make the pin indent the molded part [see eqs. (3)–(5)]. As a matter of fact, eqs. (12)–(14) also show that the indentation depth depends on the difference between the indentation pressure and the cavity pressure at the time at which the indentation is performed. The smaller the difference is, the lower the indentation depth is, as experimentally observed [Fig. 7(a)]. From eq. (14), it is also evident that if the indentation pressure equals the cavity pressure, the indentation depth must be small.

In summary, the results of Figure 7 are consistent with our interpretation of the indentation test. Furthermore, the curve calculated according to the heat-transfer model accurately fits the experimental data.

Influence of the mold temperature

Figure 8(a) shows the indentation profile for a 30% glass-fiber-reinforced PET grade at two different mold temperatures: 105 and 135°C. For this sample, a lower mold temperature leads to faster solidification. This result is in agreement with the well-known effect of the mold temperature on heat transfer within a polymer. In general, a decrease in the mold temperature leads to a faster heat transfer, which will finally result in a shorter cooling time. The same effect is observed in the normalized curves [Fig. 8 (b)], which show a faster evolution of the solidified layer as a function of time at a lower mold temperature. Again, a good agreement is found between the experimental data and the calculated curves. This illustrates that this simplified heat-transfer model is able to predict the kinetics of the solid-layer evolution only on the basis of the different mold temperatures [see eqs. (19)–(23)].

However, there is a significant difference in the end level (δ_{min}) at long cooling times for the different mold temperatures. The final level of the indentation depth at 105°C is significantly larger than the one achieved at 135°C. This result could lead to the conclusion that the final properties of the part molded at different temperatures are significantly different. According to our simplified model, this different final level must be attributed to a different compressibility of the solid, which may depend, in turn, on the crystalline content

developed in the sample. Specifically, the lower the mold temperature is, the lower the expected final crystallinity is. This experimental evidence suggests that the indentation test is sensitive not only to the kinetics of the evolution of the solid layer (especially at short cooling times) but also somehow to the final properties of the material (the final level of the indentation depth).

Effect of the holding pressure: pressure profiles in the cavity

Figure 9 shows the indentation profiles for PET samples under different holding pressures. Obviously, the experimental curves differ only for short times, whereas after 2 s, the curves tend to fall together. This observed behavior might easily be justified by the pressure traces recorded in the cavity during the injection-molding cycle. A typical pressure trace recorded for the aforementioned PET grade at an indentation time equal to zero (i.e., at the end of the packing phase) is reported in Figure 10(a). The solid curve represents the pressure trace in the cavity. In this case, the maximum recorded holding pressure is about 280 bar, corresponding to a holding pressure value set at the machine equal to 25 bar (see Table II). The dotted curve represents the indentation pressure set at the hydraulic circuit driving the indentation pin, which is set equal to 30 bar in this case. In the solid curve, a pressure spike is recorded as soon as the indentation pin penetrates into the polymer mold, confirming the hypothesis of our simplified model, which accounts for volumetric changes during the indentation. The recorded pressure in the cavity when the indentation is performed is very small, around 50 bar. This value corresponds to the value of P_1 of eqs. (4) and (5). If we look at the pressure traces for the next indentation at $t = 1$ s, reported in Figure 10(b), we may notice that the pressure profile is very similar, but the value of P_h is nearly zero. If the holding pressure is varied, obviously the shape of the curve will slightly change. Nevertheless, it is easy to conclude that after a few seconds the pressure in the cavity will be zero and then, according to eq. (13), the value of the indentation depth, depending only on the indentation pressure (which is the same for all the experiments reported in Fig. 9), must be the same for the curves. This result is clearly visible in Figure 9, in which the curves collapse on one another after the first 2 s.

A final remark can be made on the basis of the recorded pressure traces. By observing the pressure trace at $t = 0$ s, reported in Figure 10(a), one may observe that the value of the pressure spike is small (ca. 175 bar) with respect to the indentation pressure adopted (equivalent to ca. 500 bar). This leads to the conclusion that the recorded pressure spike can be used as a qualitative proof of the volumetric mechanism here proposed for the indentation. From a quan-

titative viewpoint, the pressure value recorded by the sensor depends also on the thickness of the already formed solid layer, which is in contact with the sensor itself. This is clearer in Figure 10(b) for an indentation time of 1 s; only a small pressure spike (ca. 50 bar) is visible, despite the same indentation pressure (equivalent to ca. 500 bar). The same conclusion can be stated on the basis of Figure 10(c) for an indentation time equal to 2 s; the pressure spike is not visible anymore because of the large thickness of the solid layer. Going back to the calculated solid-layer thickness according to eq. (23), one may indeed calculate from Figure 10(c) under these conditions (indentation pressure = 30 bar, holding pressure = 25 bar, mold temperature = 135°C, and indentation time = 2 s) the normalized dimensionless thickness of the solid layer, which is around 0.5. If one recalls that the half-width of the cavity is 0.8 mm, one can conclude that the thickness of the solid layer under these conditions is around 0.4 mm. This solid-layer thickness does not allow the pressure wave propagating within the sample after the indentation to be properly sensed and recorded by the pressure transducer.

These results can, however, be regarded as an indirect qualitative proof of the agreement between the experimental data and the model interpretation and simulation.

CONCLUSIONS

A special device for performing indentation experiments during the cooling stage of the injection-molding process has been designed and implemented into a standard, multipurpose injection-molding machine. From the shape of an indentation–time plot, the evolution of the solidification front as a function of time can be determined, solidification being assumed to take place abruptly as soon as T_c is reached.[5,6] A good agreement between the experimental data and predictions of the evolution of the solid-layer thickness based on the classical theory of heat penetration has been obtained. The method has been applied successfully to various PET and PBT samples and appears to be sensitive to the type of material (PET vs PBT), the molecular weight, and the operating conditions (the melting temperature, holding pressure, and indentation pressure). Therefore, this method can be regarded as a powerful tool for optimizing the operating conditions and material characteristics for injection molding and may represent a first step toward a reliable prediction of the injection-molding cycle time.

NOMENCLATURE

α	thermal diffusivity ($m^2\ s^{-1}$)
β	compressibility (bar^{-1})
β_L	compressibility of the liquid (bar^{-1})
β_S	compressibility of the solid (bar^{-1})
δ	indentation depth (mm)
δ_{max}	maximum indentation depth (mm)
δ_{min}	minimum indentation depth (mm)
δ_{norm}	normalized decrease of the indentation depth (dimensionless)
ϵ	thermal expansion coefficient (K^{-1})
ρ	density ($kg\ m^{-3}$)
c_p	specific heat ($J\ kg^{-1}\ K^{-1}$)
$dV(T,P)$	infinitesimal change in the volume
$erfc$	complementary function of the Gaussian error function
k	thermal conductivity ($W\ m^{-1}\ K^{-1}$)
K	constant
K_1	constant
l	half-thickness (m)
M_n	number-average molecular weight
P	pressure (bar)
P_i	indentation pressure (bar)
P_h	holding pressure at the time of indentation (bar)
S	cross section of the indentation pin (mm^2)
t	indentation time (s)
T	temperature (K)
T_c	crystallization temperature (K)
T_m	melting temperature (K)
T_w	wall temperature (K)
V	volume (mm^3)
V^S	volume of the solid phase (mm^3)
V^L	volume of the liquid phase (mm^3)
x	thickness of the solid layer (m)
x_S	volumetric solid fraction (dimensionless)

References

1. Guo, X.; Isayev, A. I.; Guo, L. Polym Eng Sci 1999, 39, 2096.
2. Guo, X.; Isayev, A. I.; Demiray, M. Polym Eng Sci 1999, 39, 2132.
3. Huang, T.; Kamal, M. R. Polym Eng Sci 2000, 40, 1796.
4. Brucato, V.; Piccarolo, S.; Titomanlio, G. Makromol Chem Macromol Symp 1993, 68, 245.
5. Piccarolo, S.; Saiu, M.; Brucato, V.; Titomanlio, G. J Appl Polym Sci 1992, 46, 625.
6. Brucato, V.; Crippa, G.; Piccarolo, S.; Titomanlio, G. Polym Eng Sci 1991, 31, 1411.
7. He, J.; Zoller, P. J Polym Sci Part B: Polym Phys 1994, 32, 1049.
8. Zoller, P. J Appl Polym Sci 1979, 23, 1051.
9. Zoller, P. J Appl Polym Sci 1979, 23, 1057.
10. Zoller, P.; Fakhreddine, Y. Thermochim Acta 1994, 238, 397.
11. Rastogi, S.; Newmann, M.; Keller, A. Nature 1991, 55, 353.
12. Rastogi, S.; Newmann, M.; Keller, A. J Polym Sci Part B: Polym Phys 1993, 31, 125.
13. Wunderlich, B.; Arakaw, T. J Polym Sci Part A: Polym Chem 1964, 2, 3697.
14. Tchizmakov, M. B.; Kostantinopolskaja, M. B.; Zubov, Y. A.; Bakeev, N. P.; Kotov, N. M.; Belov, G. P. Vysokomol Soedin A 1976, 18, 1121.
15. Liangbin, L.; Huang, R.; Ai, L.; Fude, N.; Shiming, H.; Chunmei, W.; Yuemao, Z.; Dong, W. Polymer 2000, 41, 6943.
16. Phillips, P. J.; Tseng, H. T. Macromolecules 1989, 22, 1649.
17. La Carrubba, V.; Brucato, V.; Piccarolo, S. Polym Eng Sci 2000, 40, 2430.
18. Brucato, V.; Piccarolo, S.; La Carrubba, V. Int Polym Proc 2000, 15, 103.
19. Choi, C.; White, J. L. Polym Eng Sci 2000, 40, 645.
20. Fleischmann, E.; Koppelmann, J. J Appl Polym Sci 1990, 41, 1115.
21. Piccarolo, S. J Macromol Sci Phys 1992, 31, 501.
22. Brucato, V.; Piccarolo, S.; Titomanlio, G. Int J Form Proc 1998, 1, 35.
23. Won, J. C.; Fulchiron, R.; Douillard, A.; Chabert, B.; Varlet, J.; Chomier, D. Polym Eng Sci 1999, 40, 2058.
24. Piccarolo, S.; Brucato, V.; Kiflie, Z. Polym Eng Sci 2000, 40, 1263.
25. Thomas, C. L.; Bur, A. J. Polym Eng Sci 1999, 39, 1291.
26. Guillet, J.; Gonnet, J. M.; Sirakov, I.; Fulchiron, R.; Seytre, G. On-line Monitoring of the Injection Moulding Process by Dielectric Spectroscopy, Proceedings of the 17th Meeting of the Polymer Processing Society, Montreal, Canada, 2001.
27. Wang, H.; Cao, B.; Jen, C. K.; Nguyen, K. T.; Viens, M. Polym Eng Sci 1997, 37, 363.
28. Brown, E. C.; Dawson, A. J.; Coates, P. D. Ultrasonic Measurements in the Nozzle and Cavity during Polymer Injection Moulding, Proceedings of the 17th Meeting of the Polymer Processing Society, Montreal, Canada, 2001.
29. Brandgrup, J.; Immergut, E. H. Polymer Handbook, 3rd ed.; Wiley: New York, 1989.
30. Thermodynamik; Hanser: Munich, 1979.
31. Isachenko, V. P.; Ossipova, V. A.; Sukomel, A. S. Heat Transfer; Mir: Moscow, 1987.
32. Pogodina, N. V.; Winter, H. H. Macromolecules 1998, 31, 8164.
33. Titomanlio, G.; Piccarolo, S.; Levati, G. J Appl Polym Sci 1988, 35, 1483.
34. Titomanlio, G.; Speranza, V.; Brucato, V. Int Polym Proc 1997, 12, 45.
35. Titomanlio, G.; Rallis, A.; Piccarolo, S. Polym Eng Sci 1988, 29, 209.
36. Gumther, B.; Zachmann, H. G. Polymer 1983, 24, 1008.